

Wednesday 25 Nov

Advances in Cryogenic Electron Microscopy for Quantum and Energy Materials

Free webinar

17.30-18.30 CET | 11.30-12.30 EST

[Register here](#)



Lena F. Kourkoutis,
Associate Professor,
Cornell University

Wiley Analytical Science

ThermoFisher
SCIENTIFIC

Tailor-Made Photoconductive Pyrene-Based Covalent Organic Frameworks for Visible-Light Driven Hydrogen Generation

Linus Stegbauer, Sebastian Zech, Gökçen Savasci, Tanmay Banerjee, Filip Podjaski, Katharina Schwinghammer, Christian Ochsenfeld, and Bettina V. Lotsch*

Covalent organic frameworks (COFs) have emerged as a new class of crystalline porous polymers displaying molecular tunability combined with structural definition. Here, a series of three conjugated, photoactive azine-linked COFs based on pyrene building blocks which differ in the number of nitrogen atoms in the peripheral aromatic units is presented. The structure of the COFs is analyzed by combined experimental and computational physisorption as well as quantum-chemical calculations, which suggest a slipped-stacked arrangement of the 2D layers. Photocurrents of up to $6 \mu\text{A cm}^{-2}$ with subsecond photoresponse times are measured on thin film samples for the first time. While all COFs are capable of producing hydrogen from water, their efficiency increases significantly with decreasing number of nitrogen atoms. The trending activities are rationalized by photoelectrochemical measurements and quantum-chemical calculations which suggest an increase in the thermodynamic driving force with decreasing nitrogen content to be the origin of the observed differences in hydrogen evolution activities.

tunability, supramolecular functionality and structural definition. COFs are formed by reversible condensation reactions under thermodynamic control, giving rise to precisely tunable framework topologies with adjustable pore dimensions.^[2] The semiconducting properties inherent to COFs, comparable to carbon nitrides^[3] and metal-organic frameworks (MOFs),^[4] make them interesting candidates for applications in optoelectronics where ordered charge percolation pathways are key,^[5,6] including photovoltaics,^[7,8] photocurrent generation,^[9] and visible-light driven photocatalysis.^[10–12] COFs based on pyrene building units show local photoconductivity,^[13] and their fluorescent backbone has been used for chemosensing by means of analyte selective fluorescence quenching.^[14] In addition,

1. Introduction

Covalent organic frameworks (COFs) constitute an emerging class of 2D and 3D porous polymers^[1] combining molecular


pyrene's extended π -system offers a unique basis for visible-light absorption as demonstrated by pyrene-derived dyes such as pyranine.^[15] Here, we present three completely planar pyrene-COFs extended by alkynes for the first time which are modulated by peripheral heteroaromatic building units. As suggested in our previous work, a planar COF backbone, resulting in an extended π -system, favorable interlayer interactions through π - π -stacking and smaller bandgaps, may play a key role in enhancing photocatalytic activity.^[10] As a result, we propose to extend both the planarity and the π -system^[11] by integrating alkyne moieties into the building blocks.

Dr. L. Stegbauer, G. Savasci, Dr. T. Banerjee, F. Podjaski,
Dr. K. Schwinghammer, Prof. C. Ochsenfeld, Prof. B. V. Lotsch
Max Planck Institute for Solid State Research
Heisenbergstr. 1, 70569 Stuttgart, Germany
E-mail: b.lotsch@fkf.mpg.de

Dr. L. Stegbauer, S. Zech, G. Savasci, K. Schwinghammer,
Prof. C. Ochsenfeld, Prof. B. V. Lotsch
Department of Chemistry
University of Munich (LMU)
Butenandtstr. 5-13, 81377 München, Germany

Dr. L. Stegbauer, Prof. B. V. Lotsch
Nanosystems Initiative Munich (NIM) & Center for Nanoscience
Schellingstr. 4, 80799 München, Germany

F. Podjaski
Ecole Polytechnique Fédérale de Lausanne
Station 12, CH-1015 Lausanne, Switzerland

 The ORCID identification number(s) for the author(s) of this article can be found under <https://doi.org/10.1002/aenm.201703278>.

© 2018 Max-Planck-Institut für Festkörperforschung. Published by WILEY-VCH Verlag GmbH & Co. KGaA, Weinheim. This is an open access article under the terms of the Creative Commons Attribution-NonCommercial License, which permits use, distribution and reproduction in any medium, provided the original work is properly cited and is not used for commercial purposes.

DOI: 10.1002/aenm.201703278

2. Results and Discussion

Three tetra-alkyne 1,3,6,8-tetraethynylpyrene building blocks – 1,3,6,8-tetrakis(4-ethynylbenzaldehyde)-pyrene (TEBPY), 1,3,6,8-tetrakis(6-ethynylnicotinaldehyde)-pyrene (TENPY), and 1,3,6,8-tetrakis(2-ethynylpyrimidin-5-carb-aldehyde)pyrene (TEPPY) (see the Supporting Information for experimental details and spectra) were designed in order to show an increasing nitrogen content in their peripheral aromatic units, entailing an increase in their electron withdrawing character. Each TEXPY monomer (X = B(enzaldehyde), N(icotinaldehyde), P(yrimidine-5-carbaldehyde) was reacted with hydrazine hydrate (120 °C, 3 d, see the Supporting Information for details) in an acetic acid catalyzed polycondensation in different aromatic solvent mixtures to yield an azine (A) connected COF as red powder (see Figure S1,

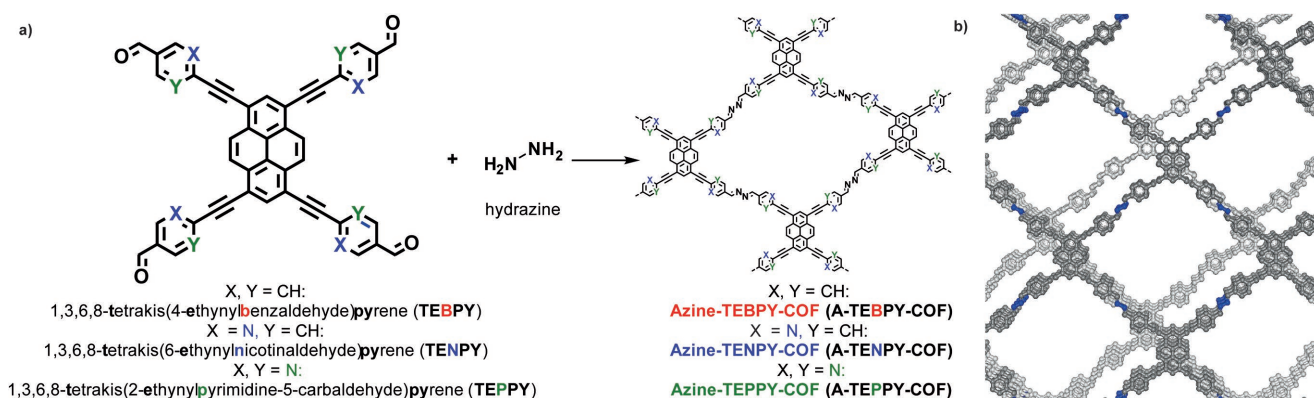


Figure 1. a) Synthesis of azine-linked COFs by the acetic acid catalyzed condensation reaction between the pyrene-based aldehyde linkers and hydrazine. b) Ball-and-stick model of the shifted AA' arrangement of A-TEBPY-COF. All COFs in this series adopt similar stackings.

Supporting Information): A-TEBPY-COF, A-TENPY-COF, and A-TEPPY-COF (Figure 1, see the Supporting Information for details and solvent screening).

Compared to the corresponding aldehydes, the A-TEBPY-COFs lack the characteristic aldehyde C–H and C=O vibrations (see Figure S7, Supporting Information) in their FT-IR spectra and show the appearance of a C=N^[16] band at 1620 cm⁻¹ (see Figure S8, Supporting Information). The CC triple bond vibration at 2200 cm⁻¹ suggests that the alkyne moiety in A-TEBPY-COFs is preserved (see Figure S9, Supporting Information).

The local structures of the A-TEBPY-COFs were further confirmed by ¹³C cross-polarization magic angle-spinning (CP-MAS) solid-state NMR spectroscopy. The disappearance of the characteristic aldehyde carbonyl ¹³C resonance located at ≈190 ppm in the precursor aldehydes is observed, along with the appearance of the azine C=N signal at ≈160 ppm (see the Supporting Information for details, see highlighted regions in blue color in Figures S8–S11, and S12 for ¹H, Supporting Information), thereby attesting the conversion of the precursors into the respective COFs. Further characterization by scanning and transmission electron microscopy (SEM, TEM resp.) shows the platelet like structure of the COF agglomerates (see Figures S48 and S49, Supporting Information). X-ray photoelectron spectroscopy (XPS) is also consistent with the formation of the framework (see Figures S50–S55, Supporting Information).

2.1. Layer Stacking and Pore Size Distribution

Powder X-ray diffraction (PXRD) reveals only moderate crystallinity for A-TEBPY and A-TENPY-COF (see Figures S2–S6, Supporting Information) with reflections at $2\theta = 4^\circ$ and 8° (see Figure 2a). Both a fully eclipsed AA-type stacking (space group *P2/m*, see Figure 2c,d), which is often employed as an idealized structure model for 2D COFs, and a layer offset of 1.6 Å as proposed for other COFs^[17,18] would be in agreement with the experimental PXRD (Figure 2a).^[17] In contrast, AB stacking can be discarded on account of a significant mismatch in intensities of the PXRD (Figure 2a).^[19]

Argon sorption isotherms at 87 K reveal the porous nature of all A-TEBPY-COFs with Brunauer-Emmett-Teller (BET) surface areas of 681 m² g⁻¹ for A-TEBPY-COF, 470 m² g⁻¹ for

A-TENPY-COF, and 920 m² g⁻¹ for A-TEPPY-COF. Interestingly, all compounds show type I isotherms characteristic of microporous materials (see Figure S14 (Supporting Information), and Figure 3a), while idealized AA or shifted (sh) 1.6 Å stacking would give rise to the formation of mesoporous pore windows of 2–2.2 nm in diameter, i.e., in the mesopore range. The observed type I isotherm may thus point to the presence of a larger layer offset or a mixture of different stacking modes, which apparently cannot be distinguished by PXRD, but may be revealed through closer inspection of the sorption isotherms and pore size distributions (PSDs). To this end, we compare two different stacking modes—a layer offset of 1.6 Å (1.6 Å-sh-AA') and a layer offset of 6.5 Å (6.5 Å-sh-AA')—based on their simulated, quenched solid density functional theory (QSDFT)-derived PSDs (Figure 3). The larger layer was exemplarily chosen based on the single-crystal X-ray structure of the related molecular building block LH₄^[20] (4-[2-[3,6,8-tris(2-(4-carboxyphenyl)-ethynyl]-pyren-1-yl)ethynyl]-benzoic acid, containing dimethylformamide (DMF) molecules, which are omitted in Figure 2b for clarity), and used to model the A-TEBPY-COF crystal structure by introducing a 6.5 Å shift between adjacent layers which were stacked in a zigzag-type pattern (see Figure 2e,f; and Figures S3 and S4, Supporting Information).^[17] Similarly large offsets have been found for other COFs such as the polyimide (PI) COFs previously.^[21] Note that similar relative intensity distributions of the eclipsed AA and the offset 1.6 Å and 6.5 Å-sh-AA' stacking modes in the simulated PXRD patterns, along with the line broadening suggest that the different offset models cannot be distinguished experimentally by PXRD (Figure 1a).

The experimental PSDs, evaluated by QSDFT (cylindrical pores, carbon), exhibit a maximum at 1.2 nm for A-TEBPY-COF, at 1.3 nm for A-TEPPY-COF, and at 1.4 nm for A-TENPY-COF (see Figure 3c; and Figure S14, Supporting Information). High-resolution TEM (HRTEM) micrographs show lattice fringes at 1.7 nm for A-TENPY-COF, in line with the expected pore size (see Figure S49, Supporting Information). Simulations^[5,22] were then performed based on the simulated sorption isotherms to extract the theoretical PSD. Here, the calculated PSD of the 6.5 Å-sh-AA' stacked structure shows the best agreement with the experimental isotherm (Figure 3c, regions marked by blue color, see the Supporting Information for details), while the

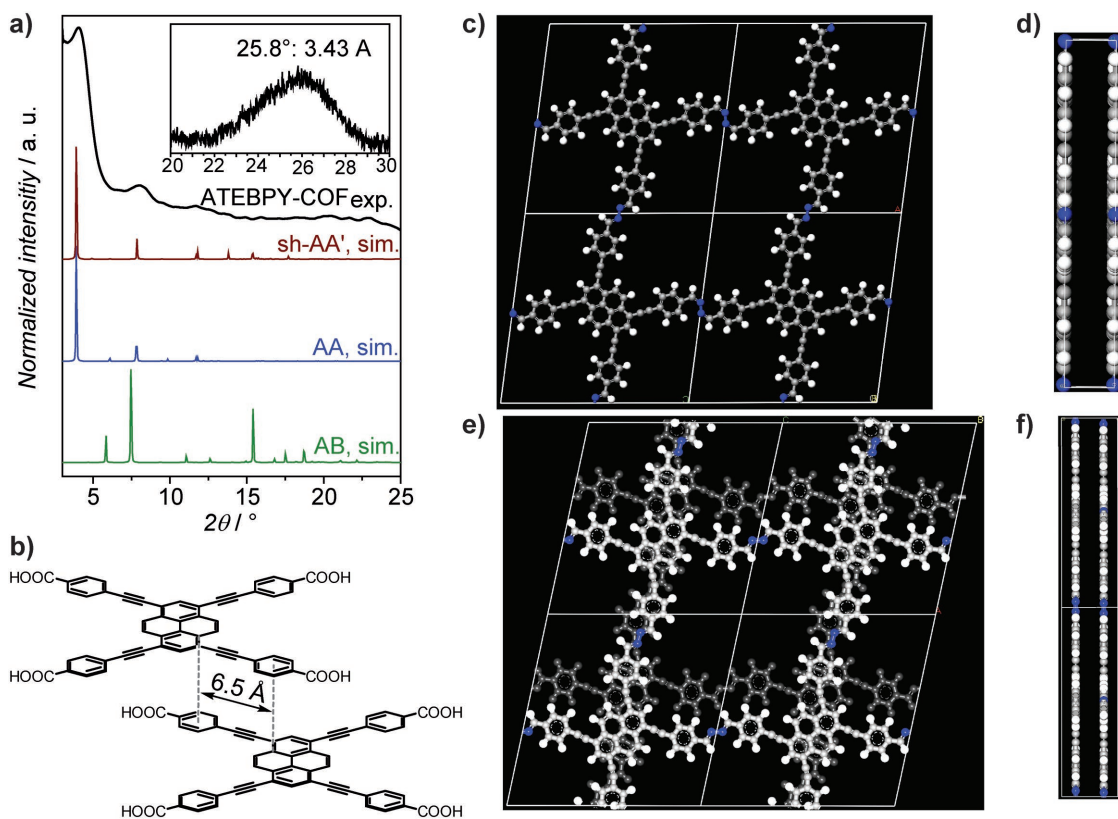


Figure 2. Characterization of A-TEBPY-COF by PXRD. a) PXRD suggests a shifted AA' or AA layer stacking. The inset shows the stacking reflection corresponding to 3.43 Å. b) Shifted stacking of pyrene units in LH_4 DMF solvate, extracted from the single-crystal X-ray structure;^[20] c, d) AA stacking of A-TEBPY-COF (gray: carbon, white: hydrogen, blue: nitrogen) e, f) hypothetical 6.5 Å shifted-AA' stacking of A-TEBPY-COF (background layer in dark grey for better visibility) Note: d, f) have not the same scale.

1.6 Å-sh-AA' stacking mode might account for the mesoporous pore volume at 2 nm (see Figure 3c regions marked by yellow color).

Next, the layer stacking modes were investigated by quantum-chemical calculations by evaluating potential energy curves of A-TEBPY-COF hexagon dimers (see Figures S28–S32 and Tables S4 and S5, Supporting Information) on the M06/def2-SVP level of theory.^[23] With a calculated layer distance of 3.40 and 3.41 Å, respectively, the resulting potential energy curves for the dimer model of both the 1.6 and 6.5 Å shifted structures are close to the experimentally observed stacking distance of 3.43 Å (see Figure 2a, inset; and Figures S29, S31, and S33, Supporting Information). In contrast, the potential energy curve for the eclipsed AA stacking mode shows a minimum at 3.69 Å, while the AB stacking mode is found to have its minimum at an unrealistically short distance of 3.00 Å (for other shifts see the Supporting Information for details).

In addition, we scanned the layer offset at a fixed stacking distance of 3.42 Å, extracted from the crystal structure of the molecular model compound LH_4 which is in close agreement to the distance observed by PXRD of A-TEBPY-COF, starting from the AA stacking mode toward and beyond the layer offset of the 6.5 Å-sh-AA' conformation. For our dimer model we find a pronounced thermodynamic minimum for the layer offset at 1.6 Å shifted from AA (see Table S5 and Figure S33 for details, Supporting Information), in line with literature.^[17]

2.2. Photoluminescence Measurements

Since the above results are inconclusive regarding the type of layer offset, we carried out photoluminescence (PL) measurements to obtain further insights into both structural and optical aspects of the COFs. PL measurements of the three materials reveal a weak, broad, and structureless excimer emission band around 670–700 nm (see Figure S17b, Supporting Information). According to literature reports, COFs with nonplanar tetra(phenyl)pyrene type linkers have a stacking distance of about 3.9 to 4.33 Å.^[14,24] In contrast, the all-planar linkers of the A-TEBPY-COFs lead to a significantly smaller stacking distance of about 3.43 Å (vide supra), hence enabling formation of excimers (see Figure S17b, Supporting Information). The TEBPY linkers in the COF thus not only result in an extended conjugation *in-plane*, but also enable electronic interactions *out-of-plane* in the form of excimers, i.e., between the COF layers, resulting in a highly redshifted emission around 670–700 nm. Note that this is the lowest energy emission ever observed in pyrene-based COFs.^[13,14,24,25]

From the photoluminescence results, a 6.5 Å shift between adjacent layers seems unlikely (see Section SH, Supporting Information): While pyrene sandwich excimers could well form by a small conformational rearrangement, i.e., a small horizontal slip, upon photoexcitation in the 1.6 Å shifted-AA' stacked system,^[26] this is unlikely for large layer offsets such as

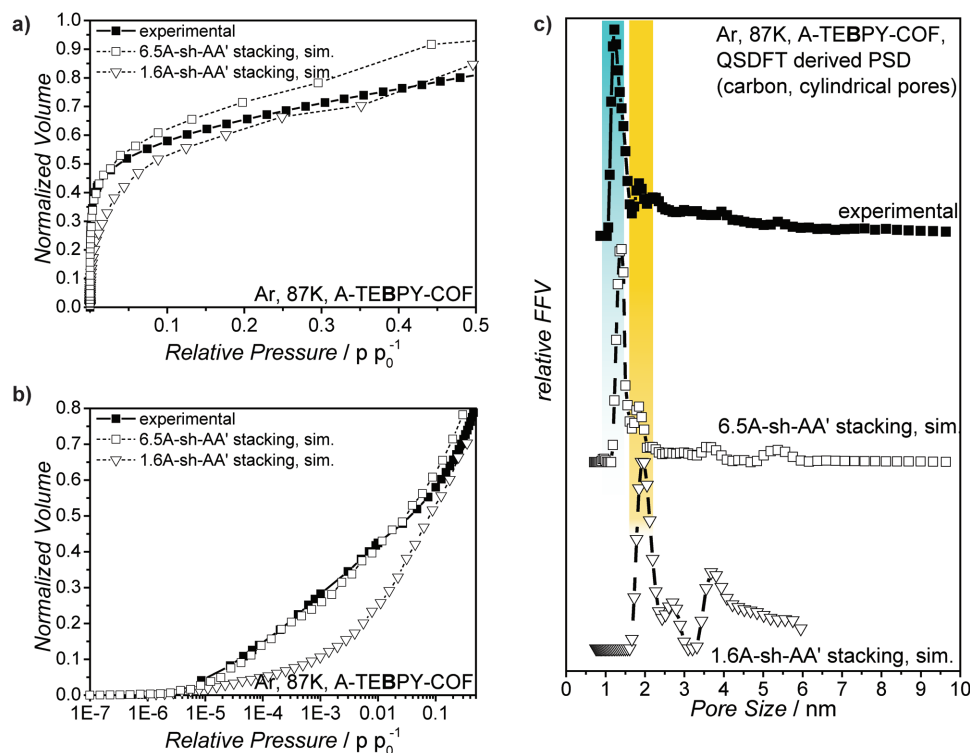


Figure 3. a) Ar isotherms at 87 K of A-TEBPY-COF, experimental (filled squares) and theoretical for 6.5 Å-sh-AA' (empty square) and 1.6 Å-sh-AA' stacking (empty triangle), with normalized volumes; b) logarithmic representation (relative pressure <math>< 0.5 p p_0^{-1}</math>) of experimental and simulated isotherms revealing microporous behavior of the experimental isotherm. c) QSDFT-derived pore size distributions of experimental and simulated Ar isotherms (carbon, cylindrical pores).

in the 6.5 Å shifted-AA' stacked system. Although in principle, a partially overlapped excimer could also be possible in the 6.5 Å-sh-AA' arrangement of the pyrene chromophores,^[27] both the PL measurements and the quantum-chemical calculations point toward smaller layer offsets represented by the 1.6 Å-sh-AA', with admixtures of larger layer offsets as revealed by PSD simulations.

2.3. Optical Properties and Photo(electro)chemistry

The diffuse reflectance UV–vis spectra of the A-TEBPY-COFs exhibit an absorption edge around 600 nm (the spike at 340 nm is due to a change of the light source), with the absorption tail extending well beyond 800 nm (Figure 4a). We estimate an optical bandgap of 1.94 eV for A-TEBPY-COF, 1.92 eV for A-TENPY-COF, and 1.91 eV for A-TEPPY-COF, based on the Tauc plot (see Figure S19, Supporting Information). Thus, the small optical bandgaps allow for the absorption of a significant portion of the solar spectrum.

A-TEBPY-COFs represent an excellent model platform for photocatalysis experiments, since compared to the previously described azine COF series^[11] the relative activities of the all-planar A-TEBPY-COFs will be dominated by their composition and electronic properties, rather than by their geometrical structures.

We thus studied light-induced hydrogen evolution by suspending the COF in phosphate buffer at pH 7.0. The mixture was

irradiated with simulated sunlight (AM 1.5 G, 100 mW cm⁻²) in the presence of in situ photodeposited platinum nanoparticles as cocatalyst for reducing the overpotential of hydrogen evolution, using 10 vol% triethanolamine (TEOA) as sacrificial electron donor (see the Supporting Information for details).^[28] Figure 4c shows a plot of the amount of hydrogen produced during a test period of 22 h for all samples (Figure 4b). All A-TEBPY-COFs steadily produce hydrogen under these conditions for at least 24 h. While A-TEBPY-COF produces hydrogen at the rate of 98 μmol h⁻¹ g⁻¹, A-TENPY-COF with 22 μmol h⁻¹ g⁻¹ falls short by a factor of 4. A-TEPPY-COF with the highest nitrogen content produced only 6 μmol h⁻¹ g⁻¹ hydrogen (Figure 4c). Analysis after 4 h under photocatalysis conditions revealed that A-TEBPY-COF shows a considerable decline in crystallinity (see Figure S20, Supporting Information) but intact local order (see Figure S21 for ¹³C ssNMR, Supporting Information).

These trends were confirmed by photocurrent density measurements in 1 M H₂SO₄ as shown in Figure 4c,d. A-TENPY and A-TEBPY-COFs were grown directly on fluorine-doped tin oxide (FTO) (see the Supporting Information for details) and illuminated with chopped, simulated sunlight. The current density of the A-TEBPY-COF (6 μA cm⁻²) at reversible hydrogen electrode (RHE) potential is approximately four times higher than the one of A-TENPY-COF (1.5 μA cm⁻²) without any cocatalyst and sacrificial donor (Figure 4c; see also Figure S24 for data in sodium phosphate buffer, Supporting Information). Chronoamperometry under visible-light irradiation at the RHE

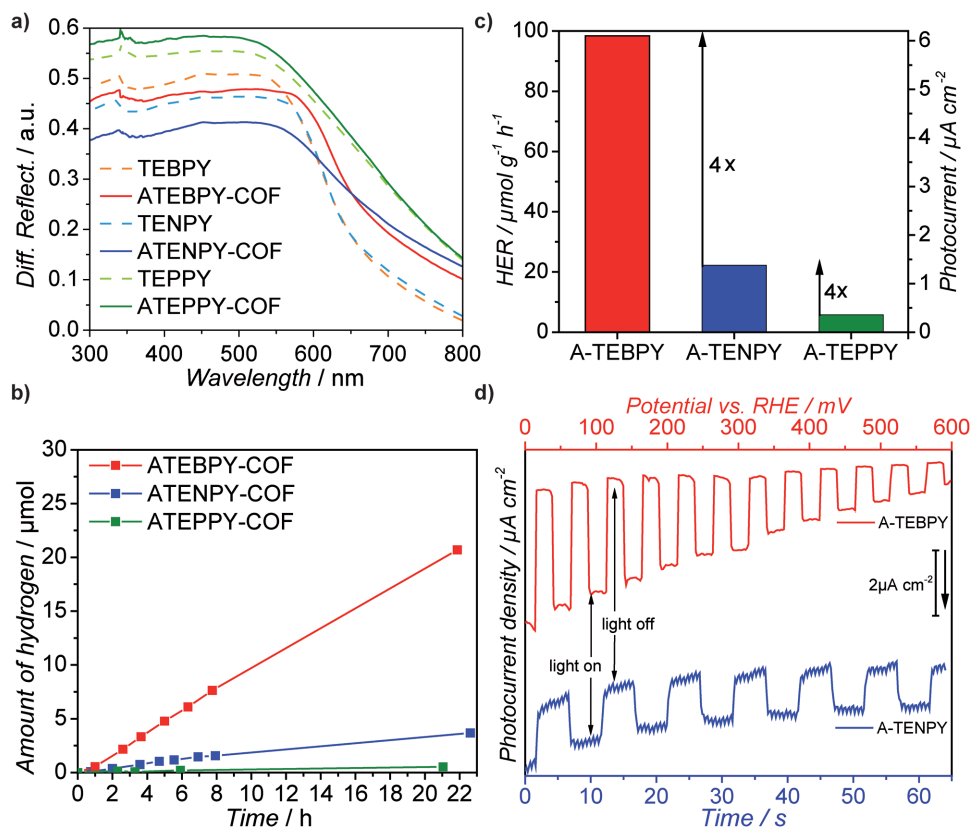


Figure 4. Optical properties of A-TEBPY-COFs, photocatalytic hydrogen evolution and photoelectrochemical characterization: a) UV-vis diffuse reflectance spectra of A-TEBPY-COFs (red, blue, green; solid lines) and their corresponding starting materials (light red, light blue, light green; dotted lines). b) Time course of photocatalytic hydrogen evolution from a 10 vol% aqueous TEOA suspension by the Pt-modified A-TEBPY-COFs under AM 1.5 G illumination. c) Comparison of the hydrogen evolution rates and photocurrents of A-TEBPY-COFs exhibiting a fourfold enhancement with decreasing nitrogen content in the peripheral aromatic unit of the system. Photocurrent densities were measured for A-TE(B,N)PY COFs@FTO under AM 1.5 G illumination at RHE potential in 1 M H₂SO₄. The photocurrents are attributed to photoelectrochemical hydrogen evolution. d) Cyclic voltammetry (top, red) and chronoamperometry (bottom, blue) measurements of the COF electrodes under chopped light. Both COFs show very fast photoresponses (<1 s).

potential (A-TENPY, Figure 4d bottom) shows the subsecond photoresponse time.

The photoresponse occurs and saturates almost instantaneously (<1 s), while the photocurrents remain stable over the measurement time, being only limited by material detachment. This is demonstrated for COFs in aqueous solution for the first time. The photoresponse at bandgap illumination as well as the stability of the photocurrents support the notion of COFs as organic semiconductors. We note that our photocurrent is at least an order of magnitude higher than other so far measured photocurrents of COFs in a nonaqueous setting.^[7,9,29] Cyclic voltammetry under visible-light irradiation (A-TEBPY-COF, Figure 4d top) shows the decrease of the photocurrents when applying a positive potential versus RHE. The anodic photoresponse occurs reproducibly over a wide range (up to 600 mV for A-TENPY and 800 mV for A-TEBPY, see Figure S23, Supporting Information) of anodic potentials versus RHE.

The decreasing photocurrent arises from a decreasing thermodynamic driving force as the valence band (VB) and conduction band (CB) levels are shifted downward with applied positive bias. This dependence was used to estimate the position of the CB in the excited state (CB_{ex}) versus RHE in 1 M phosphate buffer

and 1 M H₂SO₄ (see Figures S22 and S23, Supporting Information). A disappearing cathodic photocurrent indicates the alignment of the CB_{ex} of the COF with RHE. This is directly followed by an appearing anodic photocurrent probably arising from the oxidation of adsorbed hydrogen. Within different electrolytes this observation follows a Nernstian dependence indicating the validity of this technique (see Figures S25 and S26, Supporting Information).^[30] With a change of the electrolyte phosphate buffer (pH = 7) to H₂SO₄ (pH = 0) all energy levels drop significantly, following the chemical potential of the electrolyte (pH). The energetic positions of the conduction band in the excited state measured by this technique are shown in Figure 5a. VB levels are extrapolated by subtraction of the optical bandgap of the corresponding system.

VB and CB_{ex} energies derived by quantum-chemical calculations on PBE0-D3/def2-TZVP (see the Supporting Information for details) level of theory show a reasonable match with the photoelectrochemically derived energy levels (see Figure 5a orange lines). The brightest vertical excitations (see Tables S6–S9, and also Figures S39–S44, Supporting Information) show strong participation of the highest occupied molecular orbital (HOMO)→lowest unoccupied molecular orbital (LUMO)

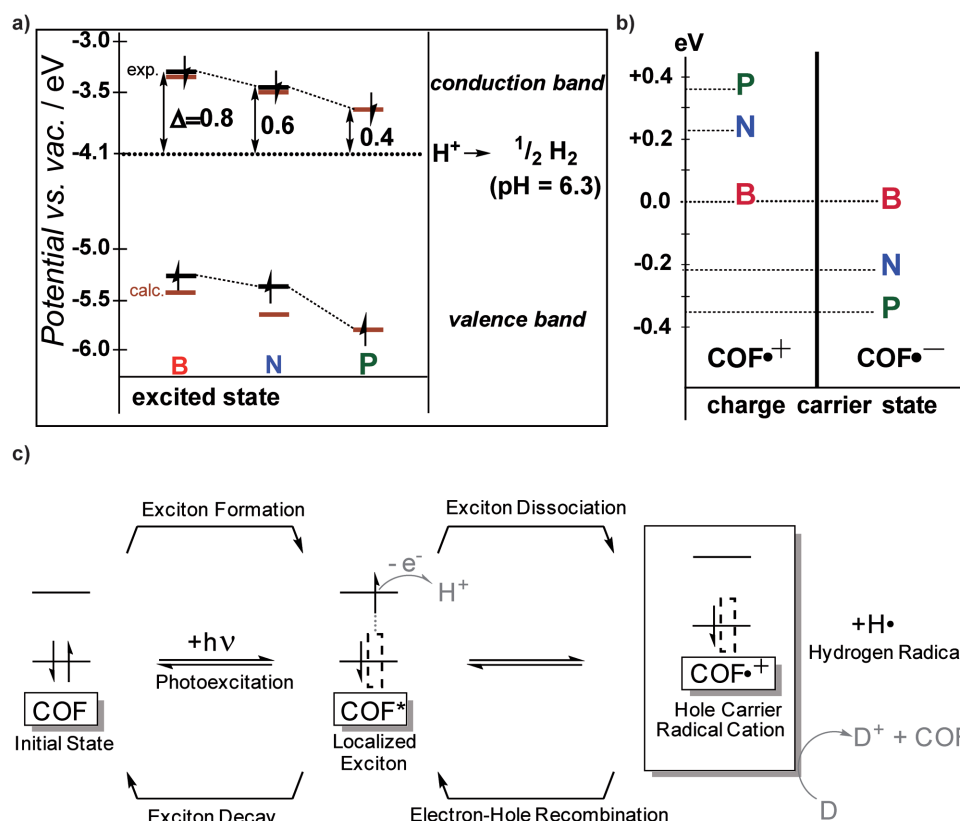


Figure 5. VB and CB alignments of the A-TEXPY-COF systems: a) Energy scheme visualizing the expected occupation and energy levels of valence and conduction band levels in the excited state of A-TEBPY, A-TENPY and A-TEPPY-COF; black lines indicate measured data obtained by photoelectrochemistry, orange lines calculated data (PBE0-D3/def2-TZVP//PBE0-D3/def2-SVP). b) Comparison of vertical radical cation and radical anion stabilization energies relative to the A-TEBPY COF system.; c) Proposed photoinduced reaction leading to the hydrogen radical and radical cation which is subsequently quenched by the sacrificial donor (D).

transition ($\approx 60\%$ for all three COFs) and are very close to the experimental values (≈ 2.10 , 2.10, and 2.11 eV compared to exp. 1.94, 1.92, and 1.91 eV for B, N, and P, respectively).

Therefore, we assign the $VB \rightarrow VB_{ex}, CB_{ex}$ ($HOMO \rightarrow HOMO_{ex}, LUMO_{ex}$) transition as crucial for photocatalysis. Electronic difference densities of this transition indicate no significant variations between the three A-TEXPY systems (see the Supporting Information). We therefore conclude that the absolute levels of the CB_{ex} are the main criteria to distinguish between the hydrogen evolution activity of those three COFs, which is in agreement with the electrochemical measurements: Excited electrons in the CB of A-TEBPY-COF have an increased thermodynamic driving force^[31] for hydrogen evolution compared to A-TENPY-COF and A-TEPPY-COF (0.8 eV against 0.5 and 0.4 eV, respectively, see Figure 5a).^[32] The computed energy levels of the CB were derived by addition of the lowest, and also brightest, vertical excitation energy to the HOMO. They match very well with the experimental ones (see Figure 5a, orange and black lines). Note that kinetic factors may play a crucial role in photocatalysis as well, but are much harder to describe by both experiment and theory. To investigate possible intermediate species during photocatalysis, we have devised a general photoexcitation scheme for the three COFs (see Figures S46 and S47, Supporting Information):^[11,31] After

excitation the exciton can either be quenched oxidatively or reductively, i.e., it can follow a radical cation or a radical anion pathway. Quantum-chemical calculations clearly show that for A-TEBPY-COF the proposed radical cation species is favored by 0.2 eV versus A-TENPY-COF and 0.4 eV versus A-TEPPY-COF, respectively (see Figure 5b left side; and Tables S10 and S11 and Figure S45, Supporting Information). The relative stability of the radical cation follows the same trend as the hydrogen evolution efficiencies—the less nitrogen in the COF, the better stabilized is the radical cation. Subsequently, this cation would be quenched by the sacrificial donor by electron donation, which closes the catalytic cycle. It is therefore conceivable that due to the increasingly electron-rich nature of the A-TEXPY-COFs along the series $X = P \rightarrow N \rightarrow B$, a radical cation pathway may operate in the photocatalytic hydrogen evolution (Figure 5c), in contrast to the N_x -COF series, which likely involves the formation of a radical anion.^[11]

Taken together, the planarity of the A-TEXPY-COFs and the extended in-plane conjugation, combined with the excimer formation in the axial direction as confirmed by the PL measurements sets the stage for the observed hydrogen evolution activity of the A-TEXPY-COF series. Trends in the hydrogen evolution reaction (HER) can be rationalized by gradual changes in the thermodynamic driving force for HER and

are consistent with a radical cation pathway, which however requires additional experimental confirmation in future studies.

3. Conclusion

In conclusion, three all-planar and conjugated azine-linked COFs were successfully synthesized by condensation of the three novel aldehyde linkers TEBPY, TENPY, and TEPPY with hydrazine. A comprehensive study based on PXRD, theoretical calculations, simulations of the pore size distribution, and photoluminescence measurements suggests the presence of stacking polytypes characterized by the prevalence of small layer offsets (<2 Å) complemented with additional larger layer offsets giving rise to microporosity. Photocatalysis experiments show significant hydrogen evolution rates for these rather electron rich systems where A-TEBPY-COF with the lowest nitrogen content and, hence, most developed donor properties, shows the highest hydrogen evolution rate. The observed trend in the photocatalytic activities is in line with an increasing thermodynamic driving force for hydrogen reduction with decreasing nitrogen content, as suggested by photocurrent measurements and quantum-chemical calculations. Subsecond photoresponse times of the COFs grown directly on FTO open up new perspectives for the potential use of these materials in optoelectronic devices. This is supported by quantum-chemical calculations indicate that the stability of the radical cation increases with decreasing nitrogen content, suggestive of an oxidative quenching mechanism. The present results further suppose that switching from p-type^[33] to n-type character of the COFs may be feasible by rational design of their molecular building blocks.

Supporting Information

Supporting Information is available from the Wiley Online Library or from the author.

Acknowledgements

B.V.L. acknowledges financial support by an ERC Starting Grant (project COFLeaf, Grant No. 639233). Financial support by the Max Planck Society, Fonds der Chemischen Industrie, FCI (scholarship for L.S.), the cluster of excellence "Nanosystems Initiative Munich" (NIM) and the Center for NanoScience (CeNS) is gratefully acknowledged. C.O. acknowledges financial support by the DFG funding initiatives SFB749 (C7) and the Excellence Cluster EXC114 (CIPSM). The authors thank Prof. T. Bein and Prof. W. Schnick for granting access to the XRD and NMR facility, C. Minke for assistance with the material analysis, Viola Duppel for TEM analysis, and Igor Moudrakovski for ssNMR measurements.

Conflict of Interest

The authors declare no conflict of interest.

Keywords

covalent organic framework, DFT calculations, photocatalysis, photocurrent, π -stacking

Received: November 21, 2017

Revised: April 20, 2018

Published online: June 28, 2018

- [1] a) G. Lin, H. Ding, R. Chen, Z. Peng, B. Wang, C. Wang, *J. Am. Chem. Soc.* **2017**, *139*, 8705; b) G. Lin, H. Ding, D. Yuan, B. Wang, C. Wang, *J. Am. Chem. Soc.* **2016**, *138*, 3302.
- [2] A. P. Côté, A. I. Benin, N. W. Ockwig, M. O'Keeffe, A. J. Matzger, O. M. Yaghi, *Science* **2005**, *310*, 1166.
- [3] a) J. Fu, J. Yu, C. Jiang, B. Cheng, *Adv. Energy Mater.* **2018**, *8*, 1701503; b) R. Shi, Z. Li, H. Yu, L. Shang, C. Zhou, G. I. N. Waterhouse, L.-Z. Wu, T. Zhang, *ChemSusChem* **2017**, *10*, 4650; c) H. Yu, R. Shi, Y. Zhao, T. Bian, Y. Zhao, C. Zhou, G. I. N. Waterhouse, L.-Z. Wu, C.-H. Tung, T. Zhang, *Adv. Mater.* **2017**, *29*, 1605148; d) H. Zhao, X. Ding, B. Zhang, Y. Li, C. Wang, *Sol. Photocatal. Energy Convers.* **2017**, *62*, 602.
- [4] a) T. Song, L. Zhang, P. Zhang, J. Zeng, T. Wang, A. Ali, H. Zeng, *J. Mater. Chem. A* **2017**, *5*, 6013; b) T. Song, P. Zhang, J. Zeng, T. Wang, A. Ali, H. Zeng, *Int. J. Hydrogen Energy* **2017**, *42*, 26605; c) H. Liu, Y. Zhao, Z. Zhang, N. Nijem, Y. J. Chabal, X. Peng, H. Zeng, J. Li, *Chem. – Asian J.* **2013**, *8*, 778; d) H. Liu, Y. Zhao, Z. Zhang, N. Nijem, Y. J. Chabal, H. Zeng, J. Li, *Adv. Funct. Mater.* **2011**, *21*, 4754.
- [5] X. Feng, L. Chen, Y. Honsho, O. Saengsawang, L. Liu, L. Wang, A. Saeki, S. Irle, S. Seki, Y. Dong, D. Jiang, *Adv. Mater.* **2012**, *24*, 3026.
- [6] S. Wan, F. Gándara, A. Asano, H. Furukawa, A. Saeki, S. K. Dey, L. Liao, M. W. Ambrogio, Y. Y. Botros, X. Duan, S. Seki, J. F. Stoddart, O. M. Yaghi, *Chem. Mater.* **2011**, *23*, 4094.
- [7] M. Dogru, M. Handloser, F. Auras, T. Kunz, D. Medina, A. Hartschuh, P. Knochel, T. Bein, *Angew. Chem., Int. Ed.* **2013**, *52*, 2920.
- [8] J. Guo, Y. Xu, S. Jin, L. Chen, T. Kaji, Y. Honsho, M. A. Addicoat, J. Kim, A. Saeki, H. Ihee, S. Seki, S. Irle, M. Hiramoto, J. Gao, D. Jiang, *Nat. Commun.* **2013**, *4*, 2736.
- [9] S. Wan, J. Guo, J. Kim, H. Ihee, D. Jiang, *Angew. Chem., Int. Ed.* **2009**, *48*, 5439.
- [10] L. Stegbauer, K. Schwinghammer, B. V. Lotsch, *Chem. Sci.* **2014**, *5*, 2789.
- [11] V. S. Vyas, F. Haase, L. Stegbauer, G. Savasci, F. Podjaski, C. Ochsenfeld, B. V. Lotsch, *Nat. Commun.* **2015**, *6*, 8508.
- [12] J. Thote, H. B. Aiyappa, A. Deshpande, D. Díaz Díaz, S. Kurungot, R. Banerjee, *Chem. – Eur. J.* **2014**, *20*, 15961.
- [13] S. Wan, J. Guo, J. Kim, H. Ihee, D. Jiang, *Angew. Chem., Int. Ed.* **2008**, *47*, 8826.
- [14] S. Dalapati, S. Jin, J. Gao, Y. Xu, A. Nagai, D. Jiang, *J. Am. Chem. Soc.* **2013**, *135*, 17310.
- [15] O. F. Mohammed, J. Dreyer, B.-Z. Magnes, E. Pines, E. T. J. Nibbering, *ChemPhysChem* **2005**, *6*, 625.
- [16] L. D. Frederickson, *Anal. Chem.* **1964**, *36*, 1349.
- [17] B. T. Koo, W. R. Dichtel, P. Clancy, *J. Mater. Chem.* **2012**, *22*, 17460.
- [18] a) X. Chen, M. Addicoat, S. Irle, A. Nagai, D. Jiang, *J. Am. Chem. Soc.* **2012**, *135*, 546; b) B. T. Koo, P. G. Berard, P. Clancy, *J. Chem. Theory Comput.* **2015**, *11*, 1172; c) J. Gao, D. Jiang, *Chem. Commun.* **2016**, *52*, 1498; d) F. Haase, K. Gottschling, L. Stegbauer, L. S. Germann, R. Gutzler, V. Duppel, V. S. Vyas, K. Kern, R. E. Dinnebier, B. V. Lotsch, *Mater. Chem. Front.* **2017**, *1*, 1354;

- e) A. Sharma, A. Malani, N. V. Medhekar, R. Babarao, *CrystEngComm* **2017**, *19*, 6950.
- [19] B. Lukose, A. Kuc, T. Heine, *Chem. – Eur. J.* **2011**, *17*, 2388.
- [20] O. V. Gutov, W. Bury, D. A. Gomez-Gualdrón, V. Krungleviciute, D. Fairen-Jimenez, J. E. Mondloch, A. A. Sarjeant, S. S. Al-Juaid, R. Q. Snurr, J. T. Hupp, T. Yildirim, O. K. Farha, *Chem. – Eur. J.* **2014**, *20*, 12389.
- [21] Q. Fang, Z. Zhuang, S. Gu, R. B. Kaspar, J. Zheng, J. Wang, S. Qiu, Y. Yan, *Nat. Commun.* **2014**, *5*, 4503.
- [22] T. C. Wang, W. Bury, D. A. Gómez-Gualdrón, N. A. Vermeulen, J. E. Mondloch, P. Deria, K. Zhang, P. Z. Moghadam, A. A. Sarjeant, R. Q. Snurr, J. F. Stoddart, J. T. Hupp, O. K. Farha, *J. Am. Chem. Soc.* **2015**, *137*, 3585.
- [23] a) Y. Zhao, D. G. Truhlar, *Theor. Chem. Acc.* **2008**, *120*, 215; b) F. Weigend, R. Ahlrichs, *Phys. Chem. Chem. Phys.* **2005**, *7*, 3297.
- [24] X. Chen, N. Huang, J. Gao, H. Xu, F. Xu, D. Jiang, *Chem. Commun.* **2014**, *50*, 6161.
- [25] a) W. Leng, Y. Peng, J. Zhang, H. Lu, X. Feng, R. Ge, B. Dong, B. Wang, X. Hu, Y. Gao, *Chem. Eur. J.* **2016**, *22*, 9087; b) J. W. Crowe, L. A. Baldwin, P. L. McGrier, *J. Am. Chem. Soc.* **2016**, *138*, 10120.
- [26] A. T. Haedler, H. Misslitz, C. Buehlmeier, R. Q. Albuquerque, A. Köhler, H.-W. Schmidt, *ChemPhysChem* **2013**, *14*, 1818.
- [27] a) F. M. Winnik, N. Tamai, J. Yonezawa, Y. Nishimura, I. Yamazaki, *J. Phys. Chem.* **1992**, *96*, 1967; b) Y. Tsujii, T. Itoh, T. Fukuda, T. Miyamoto, S. Ito, M. Yamamoto, *Langmuir* **1992**, *8*, 936; c) T. Wang, N. Zhang, K. Zhang, J. Dai, W. Bai, R. Bai, *Chem. Commun.* **2016**, *52*, 9679.
- [28] a) D. J. Martin, K. Qiu, S. A. Shevlin, A. D. Handoko, X. Chen, Z. Guo, J. Tang, *Angew. Chem., Int. Ed.* **2014**, *53*, 9240; b) S. Yang, Y. Gong, J. Zhang, L. Zhan, L. Ma, Z. Fang, R. Vajtai, X. Wang, P. M. Ajayan, *Adv. Mater.* **2013**, *25*, 2452.
- [29] M. Calik, F. Auras, L. M. Salonen, K. Bader, I. Grill, M. Handloser, D. D. Medina, M. Dogru, F. Löbermann, D. Trauner, A. Hartschuh, T. Bein, *J. Am. Chem. Soc.* **2014**, *136*, 17802.
- [30] Z. Chen, H. N. Dinh, E. Miller, *Photoelectrochemical Water Splitting: Standards, Experimental Methods, and Protocols*, Springer, New York **2013**.
- [31] P. Guiglion, E. Berardo, C. Butchosa, M. C. C. Wobbe, M. A. Zwijnenburg, *J. Phys.: Condens. Matter* **2016**, *28*, 74001.
- [32] a) A. Kudo, Y. Miseki, *Chem. Soc. Rev.* **2009**, *38*, 253; b) H. Kisch, *Angew. Chem., Int. Ed.* **2013**, *52*, 812.
- [33] T. M. Figueira-Duarte, K. Müllen, *Chem. Rev.* **2011**, *111*, 7260.